

Predicted performance of Ge/GeSn hetero-phototransistors on Si substrate at 1.55 μm

Rikmantra Basu · Vedatrayee Chakraborty ·
Bratati Mukhopadhyay · P. K. Basu

Received: 24 July 2013 / Accepted: 24 March 2014 / Published online: 2 April 2014
© Springer Science+Business Media New York 2014

Abstract Alloys of Ge and Sn grown on Si platform show about tenfold increase in the absorption over Ge at C and L-bands due to the direct nature of the band gap in GeSn. This led us to propose a Ge/GeSn/GeSn heterophototransistor (HPT) structure on a Si-platform and to calculate the terminal currents, current gain, optical gain and responsivity of the device at 1.55 μm . The model developed by Frimel and Roenker for HPTs with InGaAs base is used. In the model, the carrier density in the base is obtained by matching the diffusion-limited current with the current due to thermionic emission and tunneling across the emitter-base heterobarrier, and also considering the carrier density at the collector-end limited by the saturation drift velocity. The contribution of holes to the current is also included. The resulting carrier distribution is used to express the terminal currents and calculate the values of gain. The band gap for GeSn and the band discontinuity in the heterobarrier are calculated by using model solid theory. The calculated values for the GeSn HPT are found to be comparable with and even better than the corresponding values for the InP/InGaAs/InGaAs Npn device for lower values of the base thickness and the base doping.

Keywords Hetero junction bipolar transistor · Photodetector · Hetero-phototransistor · Electrical gain · Optical gain · Responsivity

R. Basu (✉)
EEE Department, BITS Pilani, Pilani Campus, Rajasthan 333031, India
e-mail: rikmantra.basu@pilani.bits-pilani.ac.in

V. Chakraborty · B. Mukhopadhyay · P. K. Basu
Institute of Radio Physics and Electronics, University of Calcutta,
92 Acharya Prafulla Chandra Road, Kolkata 700009, India
e-mail: vedatrayee_chakraborty@yahoo.co.in

B. Mukhopadhyay
e-mail: bmrp@caluniv.ac.in

P. K. Basu
UGC BSR Faculty Fellow, UGC, Government of India, New Delhi, India
e-mail: pkb.rpe@caluniv.ac.in

1 Introduction

Photonic devices using Si or group IV semiconductors on a Si-platform are of immense interest due to their compatibility with CMOS circuits. However, realization of such devices, especially light emitters and modulators, remained a challenge over many decades due to the indirect nature of the band gap in the materials (Deen and Basu 2012; Basu 1997). Use of Si as a photodetector material is, on the other hand, exhaustive (Deen and Basu 2012). However, Si-based detectors cannot be used in the standard telecommunication windows around 1.55 μm as the cut-off wavelength of Si is 1.1 μm . Ge-based photodetectors do not have such limitations, but growth of Ge on Si substrate poses problems due to the large lattice-mismatch between the two materials. The prospect of using a group IV semiconductor or its alloys as photodetector materials at 1.55 μm remained bleak therefore.

There is a dramatic improvement of the situation in the last 10–15 years, with the successful growth of GeSn (He and Atwater 1997) and the discovery of practical chemical vapor deposition (CVD) routes to high-quality $\text{Ge}_{1-y}\text{Sn}_y$ films and alloys of GeSiSn directly on Si substrates (Bauer et al. 2002; D'Costa et al. 2006; Roucka et al. 2008; Chizmeshy et al. 2006; Menendez and Kouvetakis 2004). The alloy $\text{Ge}_{1-y}\text{Sn}_y$ has a band gap lower than that of strained Ge, and has a larger absorption coefficient in both the C and L bands. This has led to the fabrication of the GeSn-based photodetectors (D'Costa et al. 2009; Su et al. 2011; Oehme et al. 2012; Lieten et al. 2013). The reported structures are either used as simple photoconductors (D'Costa et al. 2009; Su et al. 2011) or are grown as the usual p–i–n structures (Oehme et al. 2012).

An alternative to pin photodetectors is a Bipolar Heterojunction Photo Transistor (HPT) (Scott and Fetterman 1995; Frimel and Roenker 1997a, b; Tan et al. 2005; Abedin et al. 2004; Helme and Houston 2007; Khan et al. 2011; Park and Jang 2010; Pei et al. 2004) that offers several advantages. In addition to the compatibility of fabrication process, HPTs show optical gain without excess noise. In contrast, Avalanche Photodetectors (APDs) though have internal gain, also possess excess noise. HPTs therefore have better receiver sensitivity and signal-to-noise ratio. In the last decades, work on HPTs had been done with GaAs and InGaAs systems (Campbell 1985; Scott and Fetterman 1995; Frimel and Roenker 1997a, b). Recent years have seen a renewed interest in this device, though mainly made of III–V compounds and their alloys (Abedin et al. 2004; Tan et al. 2005; Helme and Houston 2007; Khan et al. 2011; Park and Jang 2010). There is only one reported work on SiGe alloy-based HPT (Pei et al. 2004).

In view of a large absorption coefficient of GeSn alloys, it seems worthwhile to examine the potential of HPTs based on GeSn for use at C and L bands of the optical fiber communication. In the present work, we undertake a preliminary study in this area. We have modified the earlier theory for operation of Npn bipolar HPTs, developed by Frimel and Roenker (1997a, b) based on thermionic emission of carriers across the emitter-base (EB) heterobarrier and on diffusion of electrons in the base, for the case of Ge–GeSn–Ge HPTs. The HPT is assumed to operate in the three-terminal configuration, i.e., a dc bias is applied to the base. We calculate the terminal currents, current gain and optical gain, and the responsivity of the HPT at 1.55 μm , and find that the values are comparable with those in InGaAs/InP systems. The structure considered is described in Sect. 2, the theoretical model is outlined in Sect. 3, and the results are presented in Sect. 4 and are discussed. Section 5 gives the conclusion.

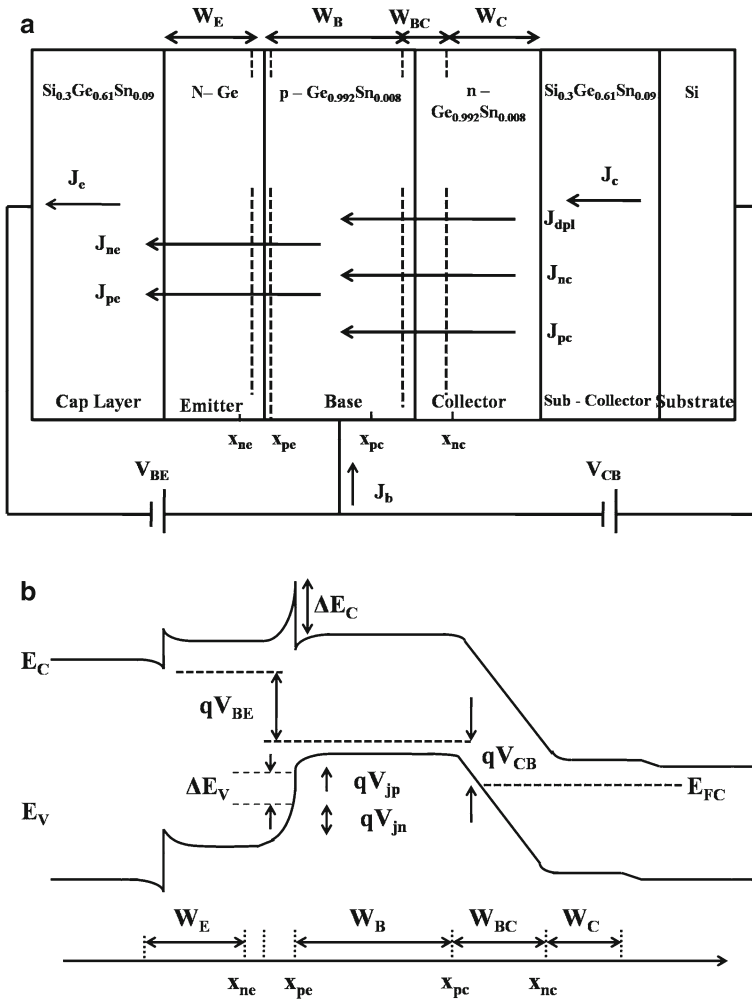


Fig. 1 **a** The schematic diagram of the Hetero Photo Transistor structure, **b** the band diagram of the Hetero Photo Transistor structure

2 HPT structure and band diagram

The three-terminal HPT device-configuration is shown in Fig. 1a, where x_{pe} and x_{pc} denote, respectively, the locations of the emitter edge and the collector edge of the quasi-neutral base region defining the effective base width, W_E , W_B and W_C are the respective widths of the emitter, base and collector regions, whereas, x_{ne} and x_{nc} are, respectively, the emitter edge of the EB depletion region and the collector edge of the BC depletion region. The corresponding energy band diagram of the HPT structure is shown in Fig. 1b.

The compositions, doping levels, widths of different regions, and different current components are also indicated in Fig. 1a. The structure is basically a heterojunction bipolar transistor (HBT) in the normal biasing mode, in which the light is directly incident at the sharp edge of the emitter-base junction, i.e., front side illumination is considered. The material combi-

Table 1 Materials for the Ge/GeSn HPT layered structure

Layer	Material	Width (μm)	Doping	Type
Cap Layer	$\text{Si}_{0.3}\text{Ge}_{0.61}\text{Sn}_{0.09}$	0.19	undoped	N
Emitter	Ge	0.2	5×10^{22}	N
Base	$\text{Ge}_{0.992}\text{Sn}_{0.008}$	0.2	7×10^{23}	p
Collector	$\text{Ge}_{0.992}\text{Sn}_{0.008}$	1	5×10^{21}	n
Sub-collector	$\text{Si}_{0.3}\text{Ge}_{0.61}\text{Sn}_{0.09}$	1.0	Undoped	n
Substrate	Si	400	Undoped	n

nation is as reported in [Oehme et al. \(2012\)](#). The compositions, doping levels and widths of different regions are listed in [Table 1](#).

The entire structure is grown on a Si substrate. The entire strain is generated on the Ge emitter layer due to the effect of the GeSn layer on the base.

3 Theoretical model

3.1 Three terminal HPT model

Theoretical models for HPTs operating in the two-terminal mode have been developed by a few workers ([Scott and Fetterman 1995](#); [Frimel and Roenker 1997a, b](#); [Tan et al. 2005](#); [Ryum and Motaleb 1990](#)). [Frimel and Roenker \(1997a, b\)](#) analyzed in more detail the operation of HPTs in the three-terminal mode. Our work follows the model by [Frimel and Roenker \(1997a\)](#) to calculate and predict the characteristics of GeSn based HPTs. We present below the essential ingredients of FR theory and quote the expressions needed for our calculation. The reader is referred to the papers by FR for detailed derivation. We assume that the incident light has a wavelength of $1.55 \mu\text{m}$.

The analysis begins with the solution of the continuity equation in the base in presence of diffusion, recombination and optical generation of carriers. Front side illumination is assumed. Plugging in the proper boundary conditions, the expressions for excess electron concentration at the ends of the neutral base, i.e., $\Delta n(x_{pe})$ and $\Delta n(x_{pc})$, are obtained, from which the electronic components of emitter and collector current densities, J_{ne} and J_{nc} , respectively, may be expressed. At the emitter end of the quasi neutral base, the excess electron density is determined by thermionic emission and tunneling across the emitter-base heterojunction ([Grinberg et al. 1984](#)). Setting equal the current density obtained from thermionic emission and tunneling with that obtained by solving the continuity equation, one arrives at an expression for $\Delta n(x_{pe})$. As is known from the analysis of BJTs or HBTs ([Neamen 1992](#); [Shur 1990](#)), $\Delta n(x_{pe})$ contains a term involving $\Delta n(x_{pc})$, which is normally set equal to the electron concentration at the collector to make the excess carrier density vanish at this end. However, [Das \(1991\)](#) pointed out the incorrectness of this approach, and accordingly [Frimel and Roenker \(1997a\)](#) used the relation $n(x_{pc}) = J_{nc}/qv_{sat}$, where v_{sat} is the saturation drift velocity. The expression for $\Delta n(x_{pe})$ is then modified and the final expressions for J_{ne} and J_{nc} , are obtained.

The total emitter current is written as $J_n = J_{ne} + J_{pe}$, where the last term denotes the contribution of holes to the emitter current density. Similarly the total collector current density is given by $J_c = J_{nc} + J_{pc} + J_{dpl}$, where the last term occurs due to absorption in the base-collector depletion layer. J_{pc} contains a dark current component J_{pc0} and a photogenerated component J_{ph} . The optical gain is given by

$$G = \frac{(\beta + 1) J_{ph}}{q F_0}, \tag{1}$$

where β is the small signal current gain, $F_0 = P_0/h\nu$ is the optical flux relating the optical power P_0 and the photon energy $h\nu$ and the photogenerated current density J_{ph} is expressed by,

$$J_{ph} = (J_{nc})_{opt} - (J_{ne})_{opt} + (J_{pc})_{opt} + J_{dpl} \tag{2}$$

The final expression for current gain is,

$$\beta = \frac{\Gamma [1 - \varphi_n \cosh(z_B)]}{\Gamma (1 + \varphi_n) [\cosh(z_B) - 1] + (\theta_n - \eta_n \varphi_n)} \tag{3}$$

where

$$\begin{aligned} z_B &= W_B/L_{nb}, \Gamma = \gamma \frac{E_{1e}}{E_{2e}} \operatorname{cosech}(z_B), \gamma = \frac{D_{nb} L_{pe} N_E}{D_{pe} L_{nb} N_B} \left(\frac{m_{nb} m_{pb}}{m_{ne} m_{pe}} \right) \exp(\Delta E_g/k_B T), \\ E_{1e} &= \cosh(z_E) + (S_e L_{pe}/D_{pe}) \sinh(z_E); E_{2e} = \sinh(z_E) + (S_e L_{pe}/D_{pe}) \cosh(z_E); \\ z_E &= W_E/L_{pe}; \theta_n = 1 + \frac{S_{dnb}}{S_{en}} \coth(z_B); \eta_n = \frac{S_{dnb}}{S_{en} \sinh(z_B)}; S_{dnb} = \frac{D_{nb}}{L_{nb}}; \\ S_{en} &\equiv v_e \gamma_n e^{(V_{jp} - \Delta E_C)/k_B T} \end{aligned} \tag{4}$$

S_{en} is the electron thermionic field emission velocity across the emitter-base heterojunction, S_e is the emitter recombination velocity at the emitter contact, ΔE_C is the conduction band discontinuity, γ_n is the added electron injection, V_{jp} is the band bending on the base side of the emitter-base heterojunction (Frimel and Roenker 1997a; Grinberg et al. 1984) and v_e is the electron thermal velocity in the emitter given by, $v_e = \sqrt{k_B T/2\pi m_n \varphi_n}$ arises from the finite electron velocity in the base-collector space charge region and is expressed as

$$\varphi_n = \frac{(S_{dnb}/v_s)}{\sinh(z_B) + (S_{dnb}/v_s) \cosh(z_B)} \tag{5}$$

The final expression for the optical gain G reads as

$$\begin{aligned} G &= \frac{\Gamma [\cosh(z_B) - \varphi_n] + (\theta_n - \eta_n \varphi_n)}{\Gamma (1 + \varphi_n) [\cosh(z_B) - 1] + (\theta_n - \eta_n \varphi_n)} \\ &\times \left\{ g_c + q \eta_c e^{-\alpha_b W_B} (1 - e^{-\alpha_c W_{BC}}) + \frac{J_{n0} \zeta_b}{n_0(x_{pc})[\theta_n - \eta_n \varphi_n]} \times \right. \\ &\left. \times \left\{ (f_{ne} \{\eta_n [\cosh(z_B) - 1] - 1\} + f_{nc} \{\theta_n [\cosh(z_B) - 1] - \varphi_n\}) \right\} \right\} \end{aligned} \tag{6}$$

Different symbols appearing in above equation are defined as follows:

$$\begin{aligned} g_c &= q \eta_c \frac{\alpha_c L_{pc}}{(\alpha_c L_{pc})^2 - 1} e^{-(\alpha_b W_b + \alpha_c W_{BC})} \times \left[\alpha_c L_{pc} - \frac{E_{2c}}{E_{1c}} - \frac{L_{pc}}{E_{1c}} \left(\alpha_c - \frac{S_c}{D_{pc}} \right) e^{-\alpha_c W_c} \right] \\ f_{ne} &= \alpha_b L_{nb} \sinh(z_B) + e^{-\alpha_b W_B} - \cosh(z_B); f_{nc} = 1 - e^{-\alpha_b W_B} [\cosh(z_B) + \alpha_b L_{nb} \sinh(z_B)]; \\ J_{n0} &= \frac{q D_{nb} n_0(x_{pc})}{L_{nb} \sinh(z_B)}; \zeta_b = \frac{\alpha_b \eta_b \tau_n}{1 - (\alpha_b L_{nb})^2} \end{aligned} \tag{7}$$

In all the above expressions, L , D and α denote, respectively, the diffusion length, diffusion constant, and absorption coefficient in the corresponding region denoted by subscripts $e(E)$, $b(B)$ and $c(C)$, the subscripts p and n refer to the conductivity type, $\eta_b(\eta_c)$ denote the optical quantum efficiency in the base (collector). The quantities E_{2c} and E_{1c} can be expressed in a similar fashion as for E_{1e} and E_{2e} given earlier by replacing the subscripts $e(E)$ in S , L , D , W by $c(C)$.

3.2 Band edges and band line-up

The average of the three valence bands is taken as the reference level. In the work, the strain dependent spin-orbit Hamiltonian has been included, in addition. Considering growth of the (001)-oriented Ge layer, lattice-matched to a relaxed $\text{Ge}_{1-x-y}\text{Si}_x\text{Sn}_y$ layer, the following expressions for the band edges of Ge are derived by using model solid theory (Menendez and Kouvetakis 2004):

$$E_{v\Gamma}(\text{Ge}) = -\frac{\Delta_0(x, y)}{3} - \Delta E_{v,av}(x, y) - \frac{\Delta_0(\text{Ge})}{6} + \delta E_h^0 + \frac{1}{4}\delta E_{001} + \frac{1}{2}\sqrt{\left(\Delta_0(\text{Ge}) + \frac{1}{2}\delta E_{001}\right)^2 + 2(\delta E'_{001})^2}, \tag{8a}$$

$$E_{c\Gamma}(\text{Ge}) = E_{v\Gamma}(\text{Ge}) + E_0(\text{Ge}) + \delta E_h^{c\Gamma} \tag{8b}$$

$$E_{cL}(\text{Ge}) = E_{v\Gamma}(\text{Ge}) + E_{ind}(\text{Ge}) + \delta E_h^{cL} \tag{8c}$$

All the energies are measured using the valence band edge of the alloy SiGeSn as the reference. Here $E_{v\Gamma}$, $E_{c\Gamma}$ and E_{cL} have the usual meanings. $E_0(\text{Ge}) = E_{c\Gamma} - E_{v\Gamma} = 0.805 \text{ eV}$ is the direct gap in Ge and $E_{ind}(\text{Ge}) = E_{cL} - E_{v\Gamma} = 0.664 \text{ eV}$ is the indirect gap in Ge. Using linear interpolation, the spin-orbit splitting in the alloy is expressed as

$$\Delta_0(x, y) = \Delta_0(\text{Ge}) - 0.26x + 0.47y, \text{ with } \Delta_0(\text{Ge}) = 0.30 \text{ eV. Also } \Delta E_{v,av}(x, y) = 0.69y - 0.48x.$$

The strain shifts are given by

$$\delta E_{001} = -2(b_1 + 2b_2) \left[\frac{2C_{12}}{C_{11}} + 1 \right] e_{II}, \delta E'_{001} = -2(b_1 - b_2) \left[\frac{2C_{12}}{C_{11}} + 1 \right] e_{II} \tag{9a}$$

$$\delta E_h^v = 2a_v \left[1 - \frac{C_{12}}{C_{11}} \right] e_{II}, \delta E_c^{c\Gamma} = 2a_c \left[1 - \frac{C_{12}}{C_{11}} \right] e_{II}, \delta E_c^{cL} = 2 \left[\Xi_d + \frac{1}{3}\Xi_u \right] \left[1 - \frac{C_{12}}{C_{11}} \right] e_{II} \tag{9b}$$

The in-plane strain is calculated from the relation

$$e_{II} = [a(\text{Ge}_{1-x-y}\text{Si}_x\text{Sn}_y) - a(\text{Ge})] / a(\text{Ge}) \tag{10}$$

where a is the lattice constant. The different strain components are evaluated by using Vegard’s law and the parameters used in the calculation are included in Tables 2 and 3.

The band edges in the ternary are calculated by using linear interpolation between the constituents. The expressions are

$$E_{c\Gamma}(x, y) = E_c(\text{Ge}) + 3.14x - 1.225y \quad \text{and} \quad E_{cL}(x, y) = E_{cL}(\text{Ge}) + 1.27x - 0.524y \tag{11}$$

4 Results and discussion

The doping densities in and the widths of the emitter, base and collector regions, as indicated in Table 1, are chosen to be equal to the values given in the paper by FR (1997a) dealing with InP/InGaAs HPTs. The values of the gain, current density, etc, obtained by FR are in agreement with the experimental values. Also no experimental data for GeSn HPTs are reported. Therefore we aim in this paper to examine how well the values for GeSn HPTs compete with the representative values for InGaAs HPTs.

Table 2 Values of parameters for alloys used in linear interpolation

Parameter	Si	Ge	Sn
Electron effective mass, m_e/m_0	0.16	0.38	0.058
Heavy hole effective mass, m_{hh}/m_0	0.49	0.28	
Light hole effective mass, m_{lh}/m_0	0.16	0.044	
Lattice constant, a (Å)	5.4307	5.6573	6.4892
Band gap, E_g (eV)			
Γ Valley	4.185	0.7985	-0.413
L Valley	1.65	0.664	0.092
Spin-orbit splitting energy, Δ_0 (eV)	0.04	0.29	0.8
Hydrostatic deformation potential at CB Γ valley	1.98	-8.24	
Hydrostatic deformation potential at CB L valley	4.18	-1.54	
Hydrostatic deformation potential at VB	2.46	1.24	
First deformation potential, b_1 (eV)	-2.35	-2.58	-2.7
First deformation potential, b_2 (eV)		-0.14	
Relative permittivity, $\epsilon(F/m)$	11.9	16.2	24
Elastic constant, C_{11} (10^{11} Pa)	1.675	128.53	
Elastic constant, C_{12} (10^{11} Pa)	0.65	48.26	
First Luttinger parameter, γ_1		13.38	-15
Second Luttinger parameter, γ_2		4.24	-11.45

In our proposed structure, the base region is a $\text{Ge}_{0.992}\text{Sn}_{0.008}$ layer (Chakraborty et al. 2013). The strain developed is 0.12% and the band edges and band discontinuities are calculated by using the parameter values listed in Tables 2 and 3. It is to be noted that we have chosen the same parameters for Ge for GeSn alloys also, when such values are unavailable for Sn. Since the concentration of Sn is very small, we believe that this approximation will not lead to much error. The values for mass, permittivity, etc, of the alloys are calculated by linear interpolation of the data for the constituent elements given in Table 2. We have used a value of 10^4cm^{-1} , for the absorption coefficient of GeSn at 0.8 eV as given by d’Costa et al. (2009). The diffusion constants correspond to the values for Ge. It is reported that the mobilities in GeSn and Ge are not different, indicating that alloy scattering is weak in GeSn alloys. The values of parameters used in the calculation are entered in Table 3.

We have first calculated the terminal current densities and the photocurrent density for the GeSn HPT. The variations of all these components are shown in Fig. 2 as a function of base-emitter voltage (V_{BE}). The nature of variation follows the same pattern for a bipolar junction transistor (BJT) or heterojunction bipolar transistor (HBT). The emitter and collector current densities show monotonic increase with increasing V_{BE} . The base current density remains constant over a range and then rises. The photocurrent density however does not show any significant variation.

The different components of the photocurrent density: the total collector current density (J_c) without recombination, the total photocurrent density (J_{ph}) and the constituent space charge region component (J_{dpl}) of photocurrent density are plotted in Fig. 3 as a function

Table 3 Values of parameters used in calculation

Effective base area	120 μm^2	Electron diffusion constant	101 $\times 10^{-4} \text{ m}^2/\text{s}$
Electron lifetime	1 ns	Hole diffusion constant	49 $\times 10^{-4} \text{ m}^2/\text{s}$
Hole lifetime	0.5 ns	Internal quantum efficiency	80%
Incident optical power	1 μW	Operating wavelength	1.55 μm
Electron saturation velocity	5 $\times 10^4 \text{ m/s}$	Emitter recombination velocity	10 m/s
Donor concentration	1.3 $\times 10^{22} \text{ m}^{-3}$	Acceptor concentration	3.7 $\times 10^{22} \text{ m}^{-3}$

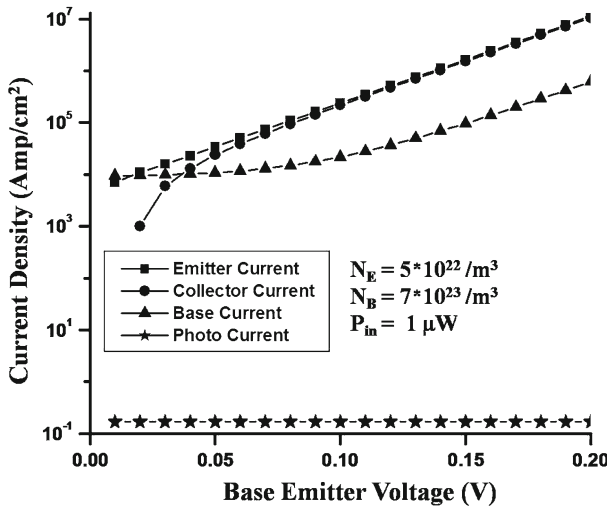


Fig. 2 Variation of terminal and photocurrent densities of GeSn HPT with base-emitter voltage [emitter current density (*black square*), collector current density (*filled circle*), base current density (*filled triangle*), and photo current density (*filled star*)] in presence of optical illumination. Recombination process dependent components are not included

of base width with a fixed base doping of $7 \times 10^{23} /\text{m}^3$. For comparison, we also include similar calculated values for InGaAs HPTs. We find that the magnitudes for total photocurrent density for GeSn device are larger than the values in InGaAs HPT. Both the curves show a decreasing trend with increasing base width. For some components of photocurrent densities, however, values for InGaAs devices are higher than the values for GeSn devices.

The total collector current is significantly larger than the photocurrent as expected, while the photo current component of space charge region is significant than the total base current due to the relatively less attenuation at the thin base region compared to emitter and collector, comparable thin size of the space charge region and small optical absorption depth ($1/\alpha_b = 1.82 \mu\text{m}$ at 1.55 μm). But the space charge region photocurrent component is much significant than the collector component (not shown in the figure). This is expected as we have considered here the front/top side illumination, and therefore the base space charge region has more exposure to light than the neutral collector located below the base region in the structure.

On the other hand, if the back side illumination is considered as in experiments, then the collector component will also have a significant value. The photocurrent components

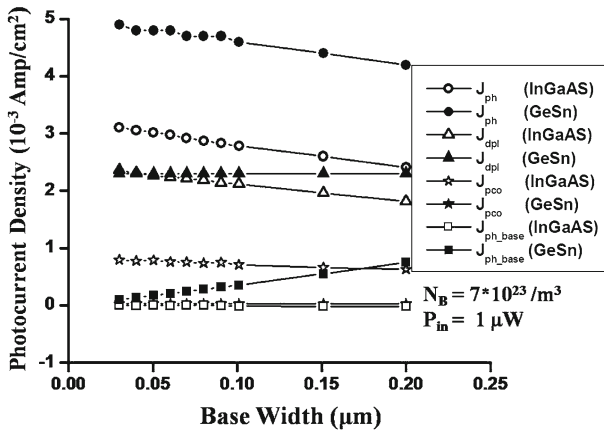


Fig. 3 Variation of total photocurrent density (J_{ph}) (filled circle GeSn; open circle InGaAs), base-collector space charge region component (J_{dpl}) (filled triangle GeSn; open triangle InGaAs), neutral base region component (J_{ph_base}) (filled star GeSn; open star InGaAs) and collector region component (J_{pco}) (filled square GeSn; open square InGaAs) with base width for a constant optical illumination of $1 \mu W$

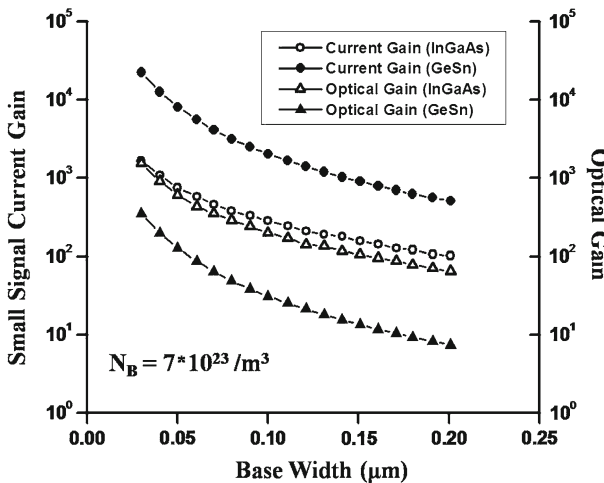


Fig. 4 Variation of optical gain (filled triangle GeSn; open triangle InGaAs) and small signal current gain (filled circle GeSn; open circle InGaAs) with base width for a constant optical illumination of $1 \mu W$ and base doping of $7 \times 10^{23} / m^3$

show slight decrease with increasing base width, since with added base absorption there is a reduction of received light intensity.

The values of optical gain and small signal current gain are plotted in Fig. 4 as a function of base width. As may be noted, the base width has a significant effect on small signal current gain; the value for $0.2 \mu m$ is reduced by more than one order from the initial value for $0.025 \mu m$. The corresponding values for InGaAs based HPTs are included in Fig. 4 for comparison. The values of current gain for GeSn structure are found to be higher than the values obtained in InGaAs HPTs (Frimel and Roenker 1997a). On the other hand, the values of optical gain are larger for InGaAs devices, the difference increasing with increase of base width.

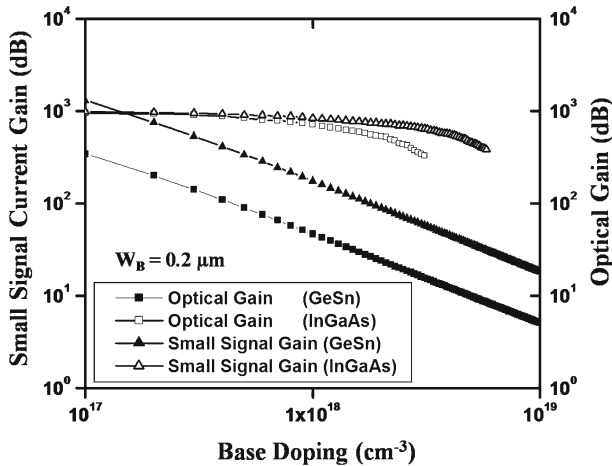


Fig. 5 Plots of optical gain (filled square GeSn; open square InGaAs) and small signal current gain (filled triangle GeSn; open triangle InGaAs) against base doping for a constant optical illumination of $1 \mu\text{W}$

The variations of optical gain and small signal current gain are now plotted in Fig. 5 as a function of base doping keeping the base width equal to $0.20 \mu\text{m}$ and optical illumination level at $1 \mu\text{W}$ for GeSn HPT. The similar data for InGaAs HPT are also included in the same figure for comparison. It is seen that both the gains show a rapidly decreasing trend with increase of base doping for GeSn device, whereas the corresponding values for InGaAs device are constant for lower values of base doping and at higher values the gains decrease slowly. It is found that the current gain is higher in the GeSn HPT for base dopings less than $1.5 \times 10^{17} \text{cm}^{-3}$. The optical gain for the GeSn device is half the value for the InGaAs device at a base doping of 10^{17}cm^{-3} . However, the rapidly increasing trend for the GeSn HPT suggests that the optical gain may exceed the values for the InGaAs device for lower base dopings.

We include in Fig. 6 plots of total photocurrent density and its various components as a function of collector width for GeSn based HPTs. All the current densities remain unchanged with increasing collector width. Similar components for device with InGaAs base are also included in the same figure. It is found that the total photocurrent density is substantially higher for GeSn device.

Figure 7 shows the effect of increase of incident front side optical power on the total photocurrent density and on the optical gain of GeSn based HPT. At lower optical power, the photocurrent density is quite low, while with increasing optical power it increases since it is directly proportional to the optical power. It can be seen to be comparable or even greater than the base current density even when HPT is biased with large dc bias.

At higher collector current densities (10^2 – 10^4Amp/cm^2), the optical gain is independent of incident optical power. It arises from the fact that the photocurrent components are directly proportional to the optical flux. Also the effects of the optically generated excess electron concentration are neglected in the base on base recombination components, which is a prime factor to make the optical gain as constant.

Figure 8 shows how the incident optical power changes the responsivity of the detector. As the power increases, responsivity decreases gradually. Here, responsivity characteristics are plotted for two base emitter voltages, 0.4 and 0.6 V, respectively. Larger the bias, larger

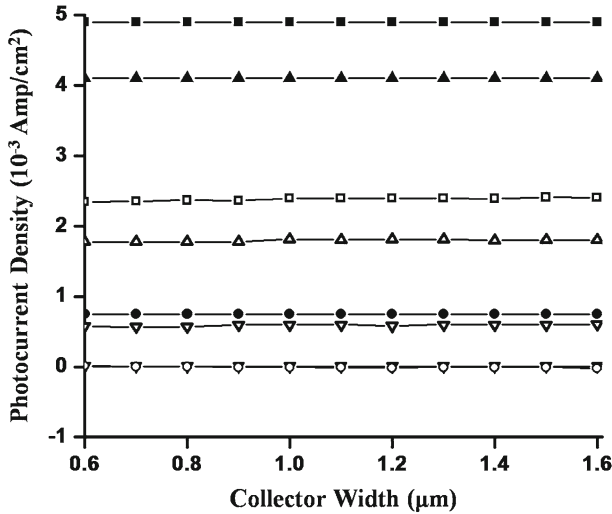


Fig. 6 Variation of total photocurrent density (*filled square* GeSn; *open square* InGaAs), base-collector space charge region component (*filled triangle* GeSn; *open triangle* InGaAs), neutral base region component (*filled circle* GeSn; *open circle* InGaAs) and collector region component (*filled inverse triangle* GeSn; *open inverse triangle* InGaAs) with collector width. The optical illumination of $1 \mu\text{W}$ and collector doping of $5 \times 10^{21}/\text{m}^3$ are assumed

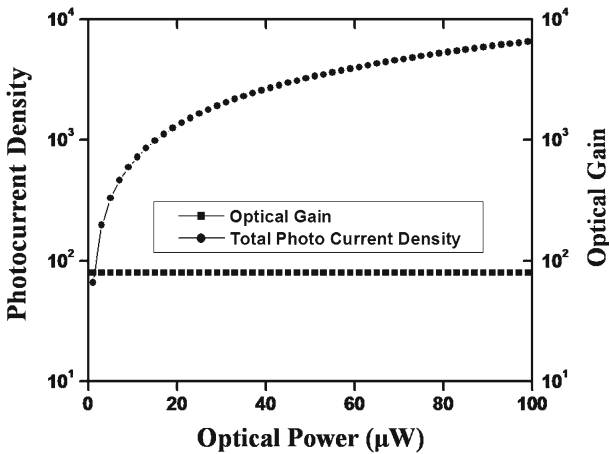


Fig. 7 Photocurrent density (*filled square*) and optical gain (*filled star*) variation with optical power

the collected current, and hence the responsivity is enhanced at the same value of incident optical power.

There is no experimental data with which our results may be compared. However as the absorption coefficient in GeSn is about two-thirds the value in InGaAs, one may expect high terminal currents for the present device. In fact the current gain and terminal currents are comparable with the InP/InGaAs HPTs (Frimerl and Roenker 1997a), and the trends indicate that the values for the GeSn HPT may even exceed the values for the InGaAs HPT for lower values of base dopings and widths.

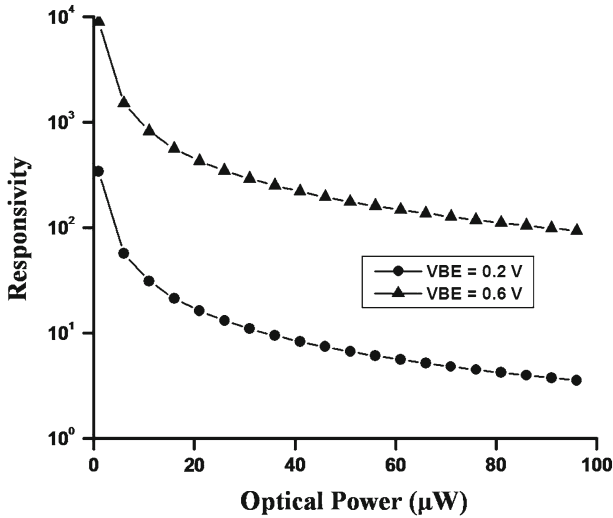


Fig. 8 Responsivity variation with optical power for two base-emitter voltages (V_{BE}): 0.2 V (filled circle) and 0.6 V (filled triangle)

5 Conclusion

We examine and predict in this paper the performance of a front side illuminated Ge–GeSn–GeSn hetero phototransistor grown on a Si platform. The strain in GeSn alloy layer makes it a direct band gap material and hence there is a drastic increase in the absorption coefficient. The terminal currents are evaluated by solving continuity equation in the base under optical generation. The current density so obtained is matched with that obtained by thermionic emission over emitter-base heterobarrier as well as tunneling through the barrier. The collector current is assumed to be limited by saturation drift velocity at the base-collector junction. The calculated values of the current gain for GeSn based HPT is higher compared with the reported values for InGaAs based HPT, but the optical gain, though lower in GeSn device, has appreciable values. The values for GeSn based HPTs are even higher for lower values of base doping and base width. The results are encouraging and may lead to practical implementation of the structure as a viable alternative to InGaAs based detectors at C and L bands of fibre optic telecommunication. The proposed structure can be grown on a Si platform.

Acknowledgments The work is partially supported by the OPERA grant awarded to the first author (Rikmantra Basu) by Birla Institute of Technology and Science (BITS) Pilani, Pilani campus, Rajasthan. Financial support for this work has also been given by the University Grants Commission (UGC) to the second author (Vedatrayee Chakraborty) under the Centre of Advance Study (CAS) Senior Research Fellowship award and to the last author (P. K. Basu) by a UGC-BSR Faculty Fellowship award.

References

- Abedin, M.N., Refaat, T.F., Sulima, O.V., Singh, U.N.: AlGaAsSb–InGaAsSb HPTs with high optical gain and wide dynamic range. *IEEE Trans. Electron Device* **51**, 2013–2018 (2004)
- Basu, P.K.: *Theory of Optical Processes in Semiconductors*. Oxford Univ. Press, UK (1997)
- Bauer, M., Taraci, J., Tolle, J., Chizmeshya, A.V.G., Zollner, S., Smith, D.J., Menendez, J., Hu, C., Kouvetakis, J.: Ge–Sn Semiconductors for band-gap and lattice engineering. *Appl. Phys. Lett.* **81**(1–3), 2992 (2002)

- Campbell, J.C.: Phototransistors for lightwave communication. In: Tsang, W.T. (ed.) *Semiconductors and Semimetals*, vol. 22, ch. 5, pp. 389–447. Academic, USA (1985)
- Chakraborty, V., Mukhopadhyay, B., Basu, P.K.: Performance prediction of an electro absorption modulator at 1550 nm using GeSn/SiGeSn quantum well structure. *Phys. E* **50**, 67–72 (2013)
- Chizmeshy, A.V.G., Ritter, C., Tolle, J., Cook, C., Menendez, J., Kouvetakis, J.: Fundamental studies of $P(\text{GeH}_3)_3$, $as(\text{GeH}_3)_3$, and $Sb(\text{GeH}_3)_3$: practical n -dopants for new group IV semiconductors. *Chem. Mater.* **18**, 6266–6277 (2006)
- Das, M.B.: HEMTs and HBTs: devices. In: Ali, F., Gupta, A. (eds.) *Fabrication and Circuits*, p. 191. Artech House, Boston (1991)
- D'Costa, V.R., Cook, C.S., Birdwell, A.G., Littler, C.L., Canonico, M., Zollner, S., Kouvetakis, J., Menendez, J.: Optical critical points of thin-film $\text{Ge}_{1-y}\text{Sn}_y$ alloys: a comparative $\text{Ge}_{1-y}\text{Sn}_y/\text{Ge}_{1-x}\text{Si}_x$ study. *Phys. Rev. B* **73**(1–16), 125207 (2006)
- D'Costa, V.R., Fang, Y., Mathews, J., et al.: Sn alloying as a means of increasing optical absorption in Ge at the C- and L- telecommunication bands. *Semicond. Sci. Technol.* **24**(1–8), 115006 (2009)
- Deen, M.J., Basu, P.K.: *Silicon Photonics: Fundamentals and Devices*. Wiley, UK (2012)
- Frimel, S.M., Roenker, K.P.: A thermionic-field-diffusion model for Npn bipolar heterojunction phototransistors. *J. Appl. Phys.* **82**, 1427–1437 (1997a)
- Frimel, S.M., Roenker, K.P.: Gummel–Poon model for Npn heterojunction bipolar phototransistor. *J. Appl. Phys.* **82**, 3581–3592 (1997b)
- Grinberg, A.A., Shur, M.S., Fischer, R.J., Morkoc, H.: An investigation of the effect of graded layers and tunneling on the performance of AlGaAs/GaAs heterojunction bipolar transistors. *IEEE Trans. Electron Dev.* **31**, 1758 (1984)
- He, G., Atwater, H.A.: Interband transitions in $\text{Sn}_x\text{Ge}_{1-x}$ alloys. *Phys. Rev. Lett.* **79**, 1937–1940 (1997)
- Helme, J.P., Houston, P.A.: Analytical modeling of speed response of heterojunction bipolar phototransistors. *IEEE J. Lightw. Technol.* **25**, 1247–1255 (2007)
- Khan, H.A., Rezaazadeh, A.A., Sohaib, S.: Modeling and analysis of the spectral response for AlGaAs/ GaAs HPTs for short wavelength optical communication. *J. Appl. Phys.* **109**(1–7), 104507 (2011)
- Lieten, R.R., Seo, J.W., Decoster, S., Vantomme, A., Peters, S., Bustillo, K.C., Haller, E.E., Menghini, M., Locquet, J.P.: Tensile strained GeSn on Si by solid phase epitaxy. *Appl. Phys. Lett.* **102**(1–5), 052106 (2013)
- Menendez, J., Kouvetakis, J.: Type-I Ge/GeSiSn strained layer heterostructures with a direct Ge band gap. *Appl. Phys. Lett.* **85**, 1175–1178 (2004)
- Neamen, D.A.: *Semiconductor Physics and Devices*. CRC Press, USA (1992)
- Oehme, M., Schmid, M., Kaschel, M., Gollhofer, M., Widmann, D., Kasper, E., Schulze, J.: GeSn p–i–n detectors integrated on Si with up to 4 % Sn. *Appl. Phys. Lett.* **101**(1–4), 141110 (2012)
- Park, M.S., Jang, J.H.: Enhancement of optical gain in floating-base InGaP–GaAs heterojunction phototransistors. *IEEE Photon. Technol. Lett.* **22**, 1202–1204 (2010)
- Pei, Z., Shi, J.W., Hsu, Y.M., Yuan, F., Liang, C.S., Lu, S.C., Hsieh, W.Y., Tsai, M.J., Liu, C.W.: Bandwidth enhancement in an integratable sige phototransistor by removal of excess carriers. *IEEE Electron Device Lett.* **25**, 286–288 (2004)
- Roucka, R., Xie, J., Kouvetakis, J., Mathews, J., D'Costa, V., Menendez, J., Tolle, J., Yu, S.Q.: $\text{Ge}_{1-y}\text{Sn}_y$ photoconductor structures at 1.55 μm : from advanced materials to prototype devices. *J. Vac. Sci. Technol. B.* **26**, 1952–1959 (2008)
- Ryum, B.R., Motaleb, I.M.A.: A Gummel–Poon model for abrupt and graded heterojunction bipolar transistors (HBTs). *Solid State Electron* **33**, 869–880 (1990)
- Scott, D.C., Fetterman, H.R.: Indium phosphide and related materials. In: Katz, A. (ed.) *Processing, Technology and Devices*, p. 351. Artech House, USA (1995)
- Shur, M.S.: *Physics of Semiconductor Devices*. Prentice-Hall, USA (1990)
- Su, S., Cheng, B., Xue, C.: GeSn p–i–n photodetector for all telecommunication bands detection. *Opt. Express* **19**, 6400–6405 (2011)
- Tan, S.H., Chen, H.R., Chen, W.T., Hsu, M.K., Lour, W.S., Lin, A.H.: Characterization and modeling of three-terminal heterojunction phototransistors using an InGaP layer for passivation. *IEEE Trans. Electron Device* **52**, 204–210 (2005)